ICAS-98-3,6,1

A98-31551

EXPERIMENTS ON DELTA WINGS WITH ROUNDED LEADING-EDGE VORTEX FLAPS

Kenichi RINOIE*
Cranfield University, Bedford MK43 0AL,
England, United Kingdom

Abstract

Low speed wind tunnel measurements were done on a 1.15m span 60° delta wing with rounded leading-edge vortex flaps. The purpose of the measurements is to assess the benefits of the rounded leading-edge vortex flaps in regard to improving the lift/drag ratio of delta wings. Force and surface pressure measurements were made at a Reynolds number based on a centreline chord of $2x10^6$. The increase in the radius of the rounded leading-edge reduces the drag significantly both with and without flap deflection except in the minimum drag region. Deflecting the rounded leading-edge vortex flap improves the lift/drag ratio at relatively higher lift coefficients, when compared with the sharp edged vortex flap. The largest improvement in the lift/drag ratio as compared with the sharp edged flat delta wing is more than 50% at a lift coefficient of about 0.6 for the rounded edge delta wing with flaps that were deflected 30° downward.

Nomenclature

b	local span, m
C_D	drag coefficient
C_L	lift coefficient
C_m	pitching moment coefficient non-dimensionalized using Cr and measured about x/Cr=0.4
Cp	pressure coefficient
Cr	wing centre-line chord, m
D	rounded leading-edge diameter, m
L/D	lift/drag ratio
U_∞	free stream velocity, m/s
x	chordwise coordinate measured from the apex of the delta wing, m
y	spanwise coordinate orthogonal to x, measured from the wing centre-line, m
α	wing angle of attack, deg
δ_f	vortex flap deflection angle measured normal to the hinge line for an original wing without leading-edge modification, deg
δ_{fc}	corrected vortex flap deflection angle for a wing with leading-edge modification, deg

Notations

SLE	sharp leading-edge
R05	rounded leading-edge D=0.005m
R15	rounded leading-edge D=0.015m
R30	rounded leading-edge D=0.03m
/n	δ_f= n (n=0° - 60°)

1. Introduction

A leading-edge vortex flap (LEVF) improves the low speed aerodynamic characteristics of a delta wing[1]. A pair of leading-edge separation vortices, which are formed over the sharp edged delta wing, produces an upward suction force that increases the drag component and consequently decreases the lift/drag ratio (Fig.1a). The LEVF is a leading-edge deflectable surface. When the LEVF is deflected downward, a leading-edge separation vortex is formed over the forward facing surface. The suction force produced by this vortex may reduce the drag component and increase the lift/drag ratio, which plays an important part in improving the take-off and climb performance of delta wing aircraft (Fig.1b). Many studies using different flap configurations have confirmed the benefit of the LEVF[2-9].

Another way to improve delta wing performance is to use a rounded leading-edge. A large fraction of the leading-edge suction force will act on the

* Visiting Research Fellow, College of Aeronautics; currently Associate Professor, Department of Aeronautics and Astronautics, University of Tokyo, 7-3-1 Hongo, Bunkyo-ku, Tokyo, 113-8656 Japan.

21st ICAS Congress
13-18 September 1998
Melbourne, Australia

rounded leading-edge and so reduce the drag component of the delta wing (Fig.1c). Numerous studies have been done in order to investigate the effects of the rounded leading-edge[10-13]. They confirmed the benefit of the rounded leading-edge but pointed out the dominance of the effect of the Reynolds number on the performance of a rounded edged wing.

These studies on the rounded leading-edge delta wings have led to the idea that a combination of LEVF and the rounded leading-edge might greatly improve the characteristics of the LEVF. By deflecting the rounded leading-edge LEVF, suction forces, which are caused both by the leading-edge separation vortex over the flap surface and by the rounded leading-edge, may reduce the drag component and increase the lift/drag ratio (Fig.1d). A previous study on the LEVF[1] by Rao investigated a delta wing with rounded leading-edges. Sharp-edged thin plates were attached to the original rounded-edge delta wing as the LEVF. The reported *L/D* improvements in Ref.1 were caused by the sharp leading-edge vortex flaps, as in Refs. 2-9.

Some preliminary wind tunnel tests[14,15] were conducted at Cranfield University in order to study the rounded edge vortex flap. A 60° rounded leading-edge delta wing model with an aerofoil section with a thickness of 10% was tested at a Reynolds number that was based on a centre line chord of 8×10^5. Although the tests were done at a relatively low Reynolds number, the results indicated positive aspects of the rounded leading-edge delta wing with a deflected LEVF as compared to a sharp edged flat delta wing. These results encouraged the author to conduct further wind tunnel tests in order to confirm the benefits of rounded LEVF. Differences in the vortex flap deflection angle and in the radius of the rounded leading-edge are believed to affect the performance of the delta wing.

Here, tests were conducted in a Cranfield 2.4 x 1.8 m low-speed wind tunnel. The 60° delta wing model[5] was again used by modifying the originally sharp leading-edge into a rounded one. The force and surface pressure measurements were made on this delta wing model with different LEVF deflection angles and with three different rounded leading-edges. Measurements were made in a range of angles of attack of -4° to +36° at the Reynolds number based on the wing centreline chord of 2×10^6.

In summary, the purpose of this study is to confirm the benefits of rounded leading-edge vortex flaps, to study the effects of the difference in the rounded leading-edge radius on wing performance and to investigate the optimum vortex flap deflection angle that gives the maximum lift/drag ratio.

2. Experimental Details

Figure 2 shows the model details. It is the same one that was tested in Ref.5, except for the leading-edge modification. The original model is a sharp edged 60° delta wing with a centre line chord length *Cr* of 1m. It has a symmetrical convex aerofoil section with a maximum thickness/chord ratio of 4.8%. The spanwise thickness distribution varies linearly from the centreline to the tip. The details of this original wing section are described in Ref.5. Two rows of pressure tappings are located on the upper surface. The model has the LEVF hinge lines running from the wing apex to 75% of the trailing-edge semispan station. Flap deflection angle δ_f is defined as the angle between the mean line of the original wing and that of the vortex flap without leading-edge modification, measured in the plane that is normal to the hinge line (see Section B-B in Fig.2). Nine different flap deflections of δ_f =0° - 60° were tested.

Rounded leading-edge modifications were made by attaching rounded leading-edge sections to the lower surface of the original wing (Fig.3). The plan shape of this section is the same as that of the vortex flap, so that the latter can be deflected. It has a constant leading-edge diameter *D* between the chordwise stations of *x/Cr*=0.3 and 0.8. The diameter is defined in the plane that is normal to the leading-edge line (see section C-C in Fig.2). This diameter decreases linearly to zero from *x/Cr*=0.3 towards the apex and from *x/Cr*=0.8 towards the trailing-edge. The thickness of this section in a spanwise direction also decreases to zero towards the flap hinge line. Three different leading-edge diameters (*D*=5mm, 15mm, and 30mm) were tested. The ratio of the rounded leading-edge radius to the root chord length is 0.25%, 0.75% and 1.5% for *D*=5mm, 15mm and 30mm, respectively. The increase in the wing area when δ_f =0°, which is caused by the attached rounded-edge sections, is 0.75%, 2.25% and 4.5% for *D*=5mm, 15mm, and 30mm, respectively. Two pressure tappings are located on the *D*=15mm and 30mm rounded leading-edge sections (Fig.3). The chordwise positions of the pressure tappings are the same as those of the main wing. Any irregularities along the intersection between the original wing and the rounded edge section were carefully blended by using Plasticine.

The experiments were made in a Cranfield 2.4m x 1.8m low-speed, closed working section, closed return wind tunnel. Most of the tests were made at a tunnel speed of U_∞=30m/s. The Reynolds number based on the wing centreline chord was 2×10^6 when U_∞=30m/s. The freestream turbulence intensity of the

K. Kondo

tunnel is about 0.09%. The model was mounted inverted from the overhead balance by a single shielded strut and a tail wire at the centre line of the tunnel. The angle of attack was in a range from -4° to +36°. Lift, drag, and pitching moment were measured using an overhead six-component electro-mechanical balance. The aerodynamic coefficients were obtained using the same tunnel boundary correction methods that were used in Ref.5. Although the main wing area increased because of the attached rounded-edge sections, all of the aerodynamic coefficients were calculated based on the original sharp edged delta wing area when δ_f =0°. The estimated overall accuracy of the coefficients is better than ±2% at 20:1 odds. Although tunnel boundary corrections were applied, accuracy at higher angles of attack is believed to decrease because of the higher tunnel wall interference. Surface pressure distributions were measured using a "Scanivalve" that was mounted within the model. The estimated overall accuracy of the pressure coefficient is ±3% at 20:1 odds. Surface pressure measurements were made for the models with rounded edges that were D=15mm and D=30mm.

The effects of the Reynolds number which is dominant for the rounded edge delta wing, as noted in Refs.10-13, is also important in the performance of the rounded edge vortex flap. Therefore, supplementary tests were made to examine the effect of the Reynolds number by increasing wind tunnel speed to U_∞=45m/s and by adding roughness strips to the leading-edge of the model. However, increasing the Reynolds number and adding roughness strips on the leading-edge of the wing did not lead to any significant level of improvement here.

Examples of the notation used in this paper are as follows. SLE/00 is the sharp leading-edge wing without any flap deflection (δ_f=0°) and R05/30 is the rounded leading-edge D=5mm with a flap deflection of δ_f=30°.

3. Results and Discussion

Prior to these measurements three component force measurements for the original sharp edged wing with δ_f=0° and 30° were repeated and compared with data from Ref.5 for the same wing configurations. The present data agree with those from Ref.5.

3.1 Three-Component Balance Measurements

Figures 4a-4e show the lift, drag, lift/drag, and pitching moment curves for three different rounded edge models with and without flap deflection (δ_f =0° and 30°) together with the results from the sharp edged wing. The C_L vs. α curves in Fig.4a show that, as the radius of the rounded edge increases, C_L decreases slightly, even though the original delta wing area is used as a reference area. Deflecting the LEVF decreases the C_L for all models, as was expected. Comparisons of the lift coefficient with 60° flat-plate delta wing data from Ref.16 are also shown in Fig.4a. In Ref.16, measurements were made using a 60°, 0.10in thickness flat-plate delta wing with beveled sharp edges at a Reynolds number of 1 million. Although there is some scattering in the results, the slope of the lift curve agrees with this data (δ_f =0°, SLE/00) until about α=25°. The discrepancy in the C_L at α=0° is caused by the presence of a shielded strut in the present measurements, as was noted in Ref.5. The discrepancy near C_{Lmax} can be attributed to vortex-bursting, as was noted in Ref.9.

Figure 4b shows the C_D vs. α curves. Increasing the radius of the leading-edge reduces C_D except in the minimum drag region. This decrease in C_D is caused in spite of the fact that the original flat delta wing area is used as a reference area. It should be noted that even the smallest increase in the rounded edge radius (R05/00 and R05/30) decreases C_D. A high suction effect of the rounded leading-edge is demonstrated. The C_L-α and C_D-α curves in Figs. 4a and 4b show decreases in C_L and C_D when the rounded leading-edge radius is increased. Similar results without LEVF deflection are seen in Ref.11 where experiments were made on 60° flat delta wings with sharp and rounded leading-edges.

Figures 4c shows the lift to drag ratio (L/D) versus C_L when δ_f =0° and 30°. Comparisons with SLE/00, R15/00 and R30/00 in Fig.4c show a limited level of improvement in the maximum L/D due to the rounded edge when δ_f =0°. However, at C_L values greater than 0.2, R15/00 and R30/00 show better L/D ratios than does SLE/00. Comparisons for the three models at δ_f =30° show no improvement in the maximum L/D due to leading-edge roundness. The maximum L/D value of R30/30 is significantly smaller than those in SLE/30 and R15/30. However, at C_L values higher than 0.5, the L/D of R30/30 shows the highest value of L/D.

In order to more clearly visualize the LEVF deflection effects on L/D, the % increase in L/D for R15, R30 and SLE/30 wings as compared with the SLE/00 wing is plotted in Fig.4d. This shows that the L/D without any flap deflection (R15/00 and R30/00) increases to more than 10% above that of the SLE/00 wing for lift coefficients greater than 0.2. The sharp edged LEVF wing (SLE/30) shows better performance

than R15/00 and R30/00 in the C_L range between 0.2 and 0.6. However, Fig.4d also shows that rounded edges with LEVF (R15/30 and R30/30) improve *L/D* more than the SLE/30 configuration for C_L values that are greater than 0.5. The most significant *L/D* improvement, which is more than 50% as compared with the sharp flat delta wing, is observed for R30/30 at about C_L=0.6

Fig.4e shows the pitching moment curves versus C_L. The LEVF and rounded edge has little effect on C_m. The aerodynamic centre position, which was measured using the C_m-C_L slope, is about 0.57*Cr* for all examples.

3.2 Surface Pressure Measurements

Figures 5 and 6 show surface pressure distribution for R15, R30 and SLE[5] in the spanwise direction for the upper surface at *x/Cr*=0.4. The spanwise coordinate is normalized by the length of the original wing local semispan. The angles of attack referred to here are those measured from the tunnel centreline and have not been corrected for tunnel wall interference. In order to clarify the effects of rounded leading-edge, pressure distributions at constant angles of attack of α=6°, 12° and 18° at *x/Cr*=0.4 are shown in Fig.5 (δ_f =0°) and Fig.6 (δ_f =30°). The formation of the leading-edge separation vortex is observed in most figures except in Fig.6a. In Fig.5a (α=6°), one can see that the suction region is present on all three wings. As the radius of the rounded edge increases, the suction peak decreases and the spanwise length of the suction region becomes shorter. A similar trend is seen at α=12° (Fig.5b). For δ_f =30° and α=6° in Fig.6a, the effects of the rounded edge is very small. However, at higher angles of attack (such as α=12° and 18°, Figs.6b and 6c) an increase in the rounded edge radius significantly reduces the spanwise length of the suction region as for δ_f =0°.

4. Effects of the Rounded Leading-Edge Radius on Different δ_f

4.1 C_P and *L/D* Distributions

In order to examine the effects of flap deflection, force and surface pressure measurements were made for nine different flap deflection angles. Figure 7 shows examples of these measurements. Surface pressure distributions for the R15 wing at a constant angle of attack α of 12° for nine different δ_f at *x/Cr*=0.4 are shown. As the vortex flap is deflected, the suction region that is over the surface of the flap shrinks and the suction region that is inboard of the flap hinge line becomes larger. These tendencies are the same as those in a previous study using a sharp leading-edge[5]. The suction pressure near the leading-edge decreases as the flap is deflected downward.

Comparisons of the three types of wings were done at a constant lift coefficient, in order to show the effects of flap deflection more clearly. Figure 8 shows the *L/D* vs. flap deflection angle at a constant C_L of 0.25 (Fig.8a) and 0.5 (Fig.8b). The data were obtained from *L/D* - C_L distribution for nine different flap deflection angles. Since the rounded leading-edge section was attached to the lower surface of the sharp edged wing, the true flap deflection angle is greater than δ_f for the R15 and R30 wings. The δ_{fc} in Fig.8 shows this corrected (true) flap deflection angle. Here, the true flap deflection angle at *x/Cr*=0.55, which is a mid chordwise station of the constant radius rounded leading-edge section (see Fig.2), is defined as δ_{fc}. The corrected vortex flap deflection angle δ_{fc} at *x/Cr*=0.55 is:

$$\delta_{fc} = \delta_f + \tan^{-1}\left(\frac{2D\sin(\varepsilon+\Lambda)}{0.55Cr\sin\Lambda} \frac{1}{\tan\left(\frac{\pi}{2}-\Lambda\right)} \right),$$

where ε is the semi-apex angle of the main wing inboard of the flap hinge line, Λ is the wing sweepback angle of 60°.

The *L/D* vs. δ_{fc} curves at C_L=0.25 in Fig.8a are similar for all three wings. However, the R15 wing had larger *L/D* for almost the entire range of δ_{fc}. The absolute maximum *L/D* at C_L=0.25 is about 12.7 when R15 and δ_{fc}=21° (δ_f =15°). The *L/D* has increased about 48% compared to the sharp edged flat delta wing at δ_{fc}=0° (i.e. SLE/00). Fig.8a also shows that the R30 wing is not as effective as the R15 wing. Figure 8b shows the *L/D* vs. δ_{fc} curves at C_L=0.5. The *L/D* vs. δ_{fc} curves are similar for the R15 and R30 wings. The maximum *L/D* at C_L=0.5 is about 7.8, which was attained for the R30 wing between δ_{fc}=32.5° and 37.5° (δ_f=20° and 25°). The % increase in *L/D* as compared with the SLE/00 is about 53%. The measurements for the original sharp edged wing were made for a limited number of examples. However, since the results in Ref.5 indicated that δ_f greater than 40° is not as effective as δ_f that is smaller than 30°, the maximum *L/D* for the sharp edged wing at C_L=0.5 was attained near δ_f =30°. The maximum % increase in *L/D* (as compared with SLE/00) is about 40% when δ_f =30° (SLE/30). This means that the rounded leading-edge vortex flaps are more effective than the sharp edged vortex flaps at relatively high lift coefficients (C_L=0.5).

4.2 Optimum *L/D* Condition

Figure 9a shows pressure distribution for three wings (R15, R30 and SLE[5]) when the absolute maximum *L/D* was attained for each wing. Here, the maximum *L/D* that was attained for each wing is called the absolute maximum *L/D*. It should be noted that the absolute maximum *L/D*, which corresponds to the true peak in the *L/D* curve, is difficult to accurately evaluate, because the true peak in the *L/D* curve often lies between two of the data points, as was noted in Ref.9. Here, the observed maximum *L/D* configurations from Fig.4c were used to discuss the pressure distributions. As was discussed in Ref.5, the maximum *L/D* for the sharp edged wing is attained when the flow attaches on the flap surface without forming a large separation vortex. Fig.9a shows that, for the R15 and R30 wings, only a small suction region at the leading-edge is observed. Therefore, the absolute maximum *L/D* for the rounded edged wing with a vortex flap is attained at flow conditions similar to those for the sharp edged wing, when there is only a small separated region and no large separation vortex on the surface of the flap. Traub[17] discussed the effects of vortex flaps and the rounded leading-edge separately. It deduced that the maximum *L/D* for the rounded LEVF wing is attained when separation over the surface of the flap is suppressed. Present results are similar to those deduced in Ref.17. In Fig.9a, the numerical values of the maximum *L/D* for each of the three wings are also shown. Use of the rounded-edge did not improve the maximum *L/D*.

Fig.9b shows the pressure distributions when the local maximum *L/D* is attained at a constant C_L of 0.5 for the three wing configurations. The local maximum *L/D* is the maximum *L/D* that was chosen from the data when the measured C_L is almost equal to 0.5. The local maximum L/D configuration was obtained from Fig.8b. Since the pressure measurements were made at a specific angle of attack without taking C_L into account, the *Cp* distributions when C_L is the closest to the constant value of 0.5 are shown. The *Cp* distributions in Fig.9b show that a separation vortex is formed on the surface of the vortex flap for all three configurations. The spanwise length of the vortex for the SLE/30 is very similar to the length of the flap span. As the radius of the rounded leading-edge increases, the suction peak of the vortex decreases.

5. Axial Force Distributions

Figure 10 shows axial force coefficients C_A versus C_L curves. C_A is defined by

$$C_A = C_D \cos\alpha - C_L \sin\alpha.$$

The negative value of C_A is caused not only by the leading-edge suction force but also by suction pressure acting on the positive slope area on the upper rounded surface near the leading-edge. The SLE/00 wing has a small negative value of C_A at C_L values higher than 0.3. However, the suction component of C_A for the R15/00 and R30/00 wings is much larger than the SLE/00. Figure 10 also shows the results from Ref.11. The tests in Ref.11were made on 60° flat-plate delta wings that had sharp and rounded leading-edges. The models used have a maximum thickness to local chord ratio of 3%. The rounded leading-edge radius which was normalized by the local chord length is 1.582%, which is almost equivalent to the R30/00 model used in this study. Measurements were made at a Reynolds number which was based on a mean chord of $1.6\text{x}10^6$. The C_A curves of Ref.11 show similar distributions to those of present measurements for δ_f =0° wings. As the radius of the leading-edge increases, the negative value of C_A increases at a higher C_L.

The C_A distributions for the wing with vortex flaps show that a strong suction force is acting on the wing at C_L values higher than 0.2, even for the sharp edge wing (SLE/30). The minimum C_A in this figure is attained for the R30/30 wing. This corresponds to the fact that the R30/30 attained the maximum *L/D* at C_L values higher than 0.5 in Fig.4c. It is significant that the sharp-edged wing with vortex flaps (SLE/30) achieves almost the same axial suction force as that of the rounded leading-edge flat delta wing (R30/00) at C_L higher than 0.7.

According to these results, benefit of the rounded leading-edge can be clearly seen at relatively high lift coefficients (C_L greater than 0.5). The surface pressure measurements in Figs. 5, 6, and 9b indicated that the spanwise length of the suction region, which was formed on the surface of the flap, was reduced and the suction peak decreased, as the radius of the rounded edge increased. These effects on the rounded leading-edge might be related to the improvement in *L/D* at C_L values greater than 0.5.

In this study, the benefits of a rounded leading-edge vortex flap at low speed were investigated. Research on rounded leading-edge vortex flaps at supersonic speeds is an important topic, because delta wing aircraft often fly at supersonic speeds.

6. Conclusions

Force and surface pressure measurements were made using a 1.15m span 60° delta wing model at the Reynolds number that was based on the centreline

L. RINOIE

chord of $2x10^6$ to investigate the effects of a rounded leading-edge with and without vortex flaps.

1) The increase in the radius of the rounded leading-edge reduces the drag significantly both with and without flap deflection except in the minimum drag region. The increase in the radius of the rounded leading-edge reduces the spanwise length of the suction pressure region on the surface of the flap.

2) A rounded leading-edge delta wing without any vortex flap deflection affords approximately a 10% improvement in lift/drag ratio relative to the sharp edged flat delta wing at lift coefficients greater than 0.2.

3) Deflecting the rounded leading-edge vortex flap improves the lift/drag ratio as compared with the sharp edged vortex flap at relatively high lift coefficients (C_L values greater than 0.5). The greatest percentage improvement in the lift/drag ratio as compared with the sharp edged flat delta wing is more than 50% at a lift coefficient of 0.6 for a 30° flap deflection angle with a 30mm diameter rounded leading-edge vortex flap.

4) The absolute maximum lift/drag ratio for the rounded edge wing with the vortex flap deflection is achieved when there is no large area of separation over the deflected vortex flap surface; this agrees with the observations made for the sharp edged delta wing. However, the absolute maximum lift/drag ratio for the rounded edge wing was not improved when compared with the sharp edged wing.

Acknowledgments

The author expresses his gratitude to Prof. J. L. Stollery, College of Aeronautics for his beneficial advice. He also expresses his gratitude to members of the workshop in the College of Aeronautics for their help in performing the wind tunnel tests.

References

1) Rao, D.M., "Leading Edge Vortex-Flap Experiments on a 74deg. Delta Wing," NASA CR-159161, Nov. 1979.
2) Marchman III, J.F., "Effectiveness of Leading-Edge Vortex Flaps on 60 and 75 Degree Delta Wings," *Journal of Aircraft*, Vol.18, No.4, 1981, pp.280-286.
3) Hoffler, K.D. and Rao, D.M., "An Investigation of the Tabbed Vortex Flap", *Journal of Aircraft*, Vol.22, No.6, 1985, pp.490-497.
4) Frink, N.T., "Subsonic Wind-Tunnel Measurements of a Slender Wing-Body Configuration Employing a Vortex Flap," NASA TM-89101, Jul. 1987.
5) Rinoie, K. and Stollery, J.L., "Experimental Studies of Vortex Flaps and Vortex Plates," *Journal of Aircraft*, Vol.31, No.2, 1994, pp.322-329.
6) Levin, D. and Seigner, A., "Experimental Investigation of Vortex Flaps on Thick Delta Wings", *Journal of Aircraft*, Vol.31, No.4, 1994, pp.988-991.
7) Traub, L.W., "Aerodynamic Characteristics of Vortex Flaps on a Double-Delta Planform," *Journal of Aircraft*, Vol.32, No.2, 1995, pp.449-450.
8) Deng, Q. and Gursul, I., "Effect of Leading-Edge Flaps on Vortices and Vortex Breakdown", *Journal of Aircraft*, Vol.33, No.6, 1996, pp.1079-1086.
9) Rinoie, K. and et al., "Experimental Studies of a 70-Degree Delta Wing with Vortex Flaps," *Journal of Aircraft*, Vol.34, No.5, 1997, pp.600-605.
10) Jones, R., Miles, J.W. and Pusey, P.S., "Experiments in the Compressed Air Tunnel on Swept-back Wings Including Two Delta Wings," British Aeronautical Research Council (A.R.C.) R.&M. 2871, 1954.
11) Fletcher, H.S., "Low-Speed Experimental Determination of the Effects of Leading-Edge Radius and Profile Thickness on Static and Oscillatory Lateral Stability Derivatives for a Delta Wing," NACA TN-4341, Jul., 1958.
12) Henderson, W.P., "Effects of Wing Leading-Edge Radius and Reynolds Number on Longitudinal Aerodynamic Characteristics of Highly Swept Wing-Body Configurations at Subsonic Speeds," NACA TN D-8361, Dec. 1976.
13) Chu, J. and Luckring, M., "Experimental Surface Pressure Data Obtained on 65° Delta Wing Across Reynolds Number and Mach Number Ranges," NASA TM 4645, Feb. 1996.
14) Hu, B.K. and Stollery, J.L., "The Performance of 60° Delta Wings: The Effects of Leading Edge Radius and Vortex Flaps," College of Aeronautics Rept. No.9004, Cranfield Inst. of Technology, Bedford, England, UK, Mar. 1990.
15) Rinoie, K., "Low Speed Aerodynamic Characteristics of 60° Rounded Leading-Edge Delta Wing with Vortex Flaps: Part 1. 457.2mm Span Delta Wing," College of Aeronautics Rep. No.9611, Cranfield Univ., Bedford, England, UK, Dec. 1996.
16) Wentz, Jr, W.H. and Kohlman, D.L., "Vortex Breakdown on Slender Sharp-Edged Wings," *Journal of Aircraft*, Vol.8, No.3, 1971, pp.156-161.
17) Traub, L.W., "Comparative Study of Delta Wings with Blunt Leading Edges and Vortex Flaps," *Journal of Aircraft*, Vol.33, No.4, 1996, pp.828-830.

K. RINOIE

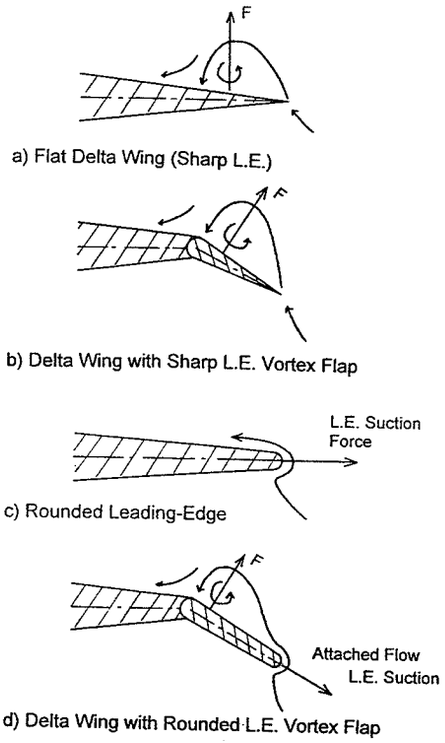

Fig.1 Concept of Vortex Flap & Rounded L.E.

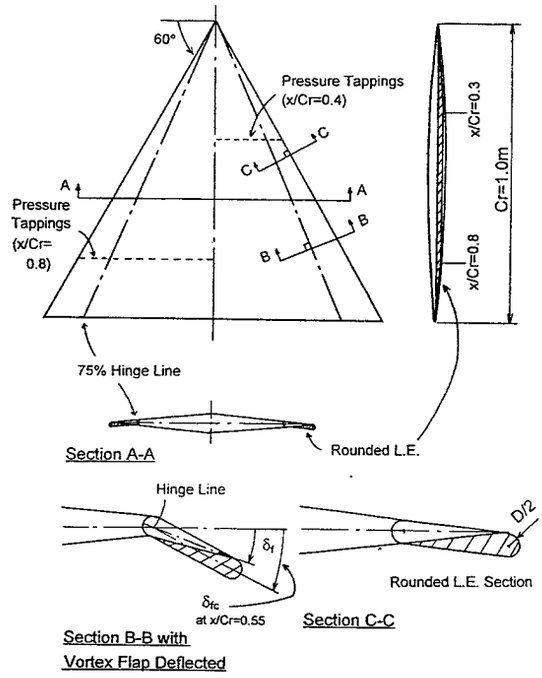

Fig.2 Delta Wing Model with Rounded L.E. LEVF

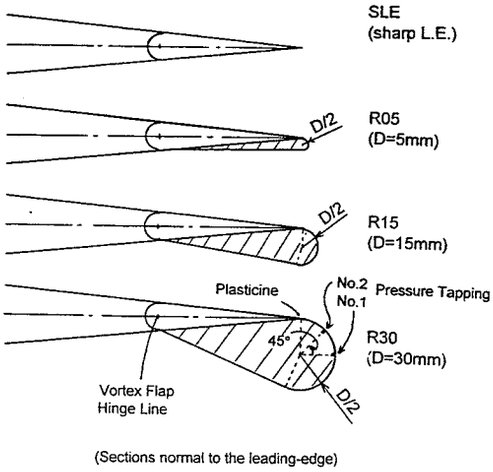

Fig.3 Different Rounded Leading-Edges

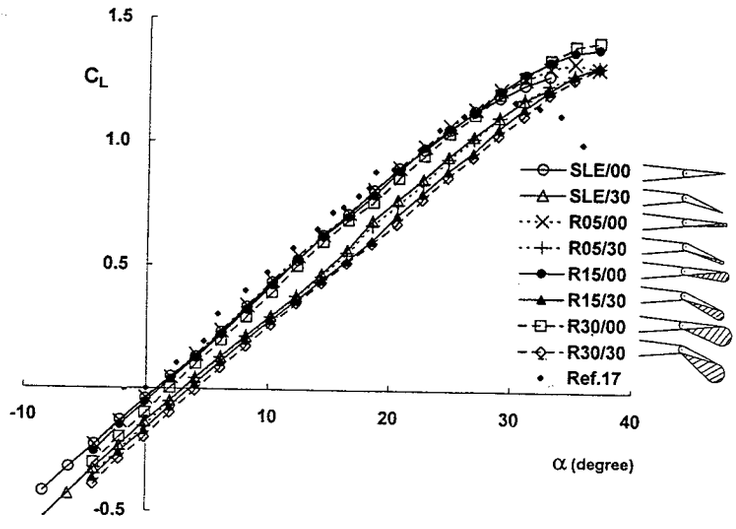

Fig.4a) C_L-α

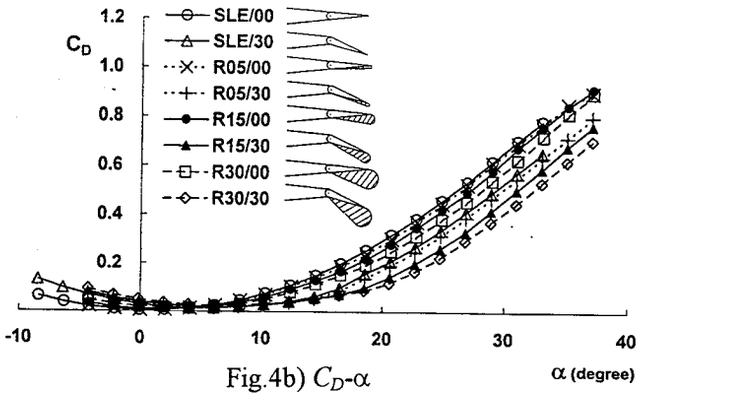

Fig.4b) C_D-α

Fig.4 Effects of Rounded L.E. with and without flap deflection

K. RINOIE

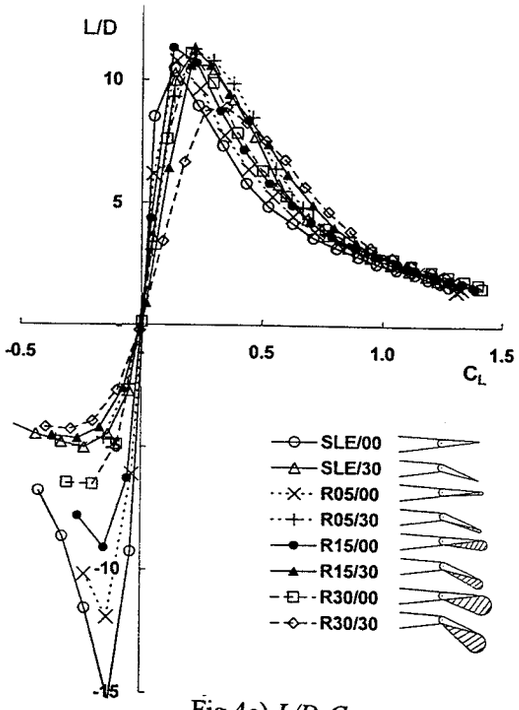

Fig.4c) L/D-C_L

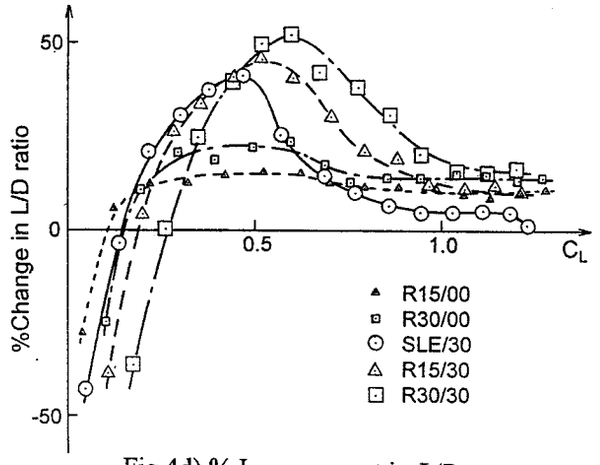

Fig.4d) % Improvement in L/D

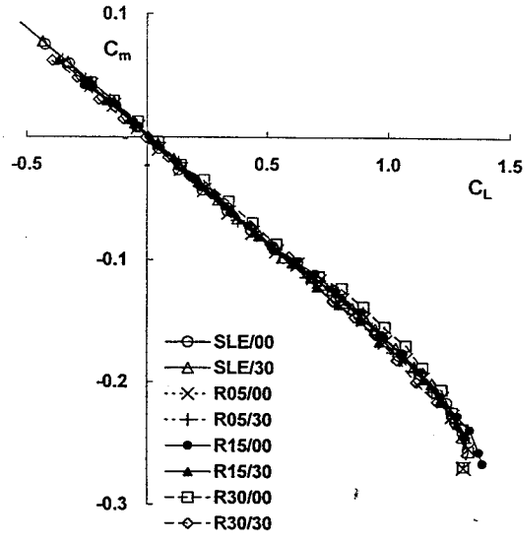

Fig.4e) C_m-C_L

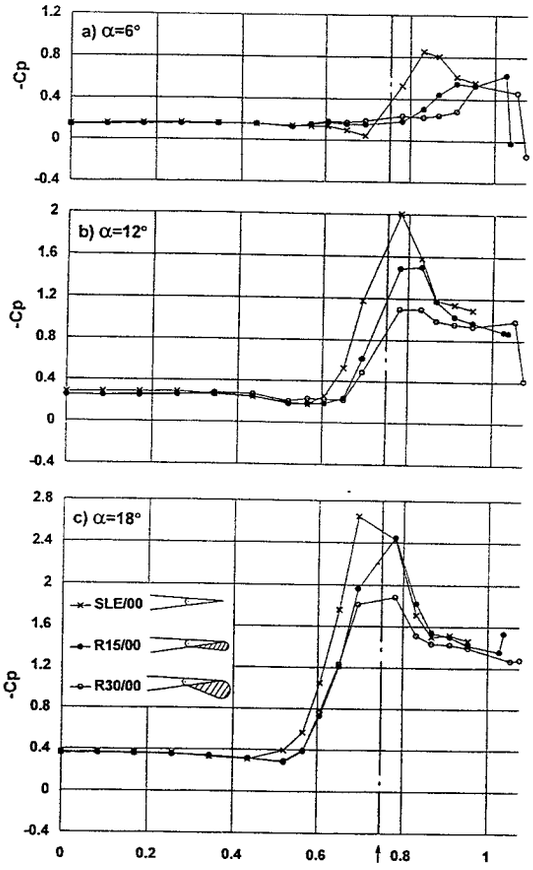

Fig.5 Surface Pressure Distribution at constant α (δ_f=0°)

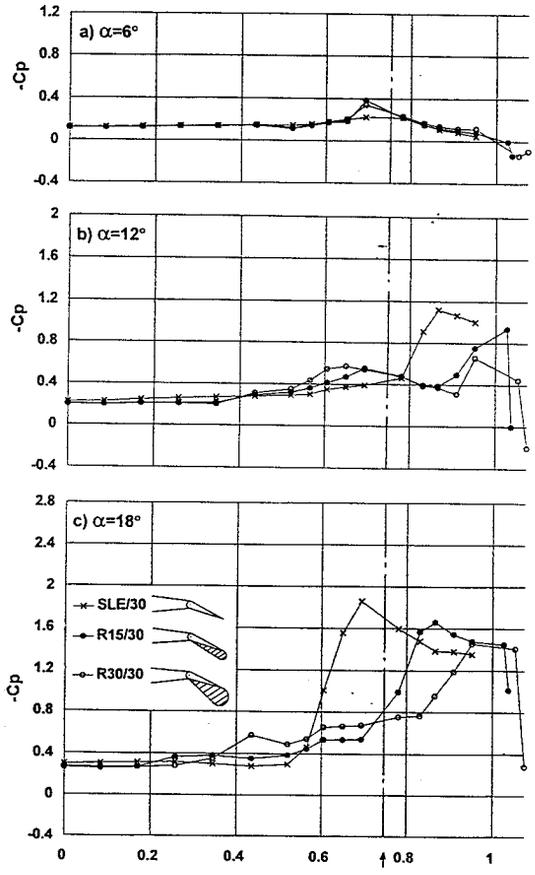

Fig.6 Surface Pressure Distribution at constant α (δ_f=30°)

K. RINOIE

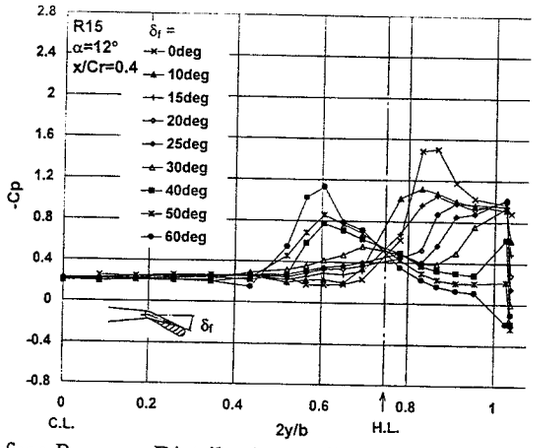

Fig.7 Surface Pressure Distribution at different δ_f (R15, α=12°)

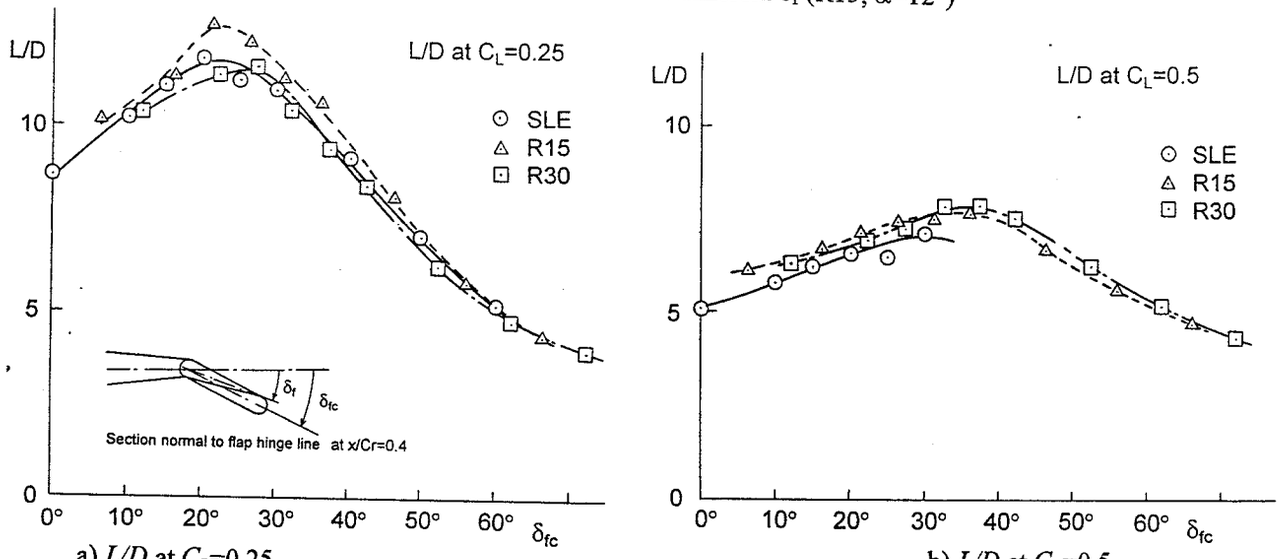

a) L/D at C_L=0.25 b) L/D at C_L=0.5

Fig.8 L/D vs. Corrected δ_f at Constant C_L

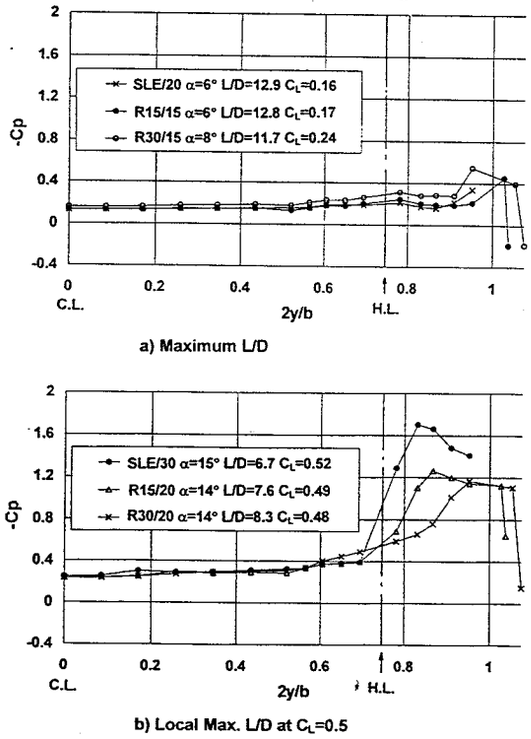

Fig.9 Surface Pressure Distribution for optimum L/D configurations

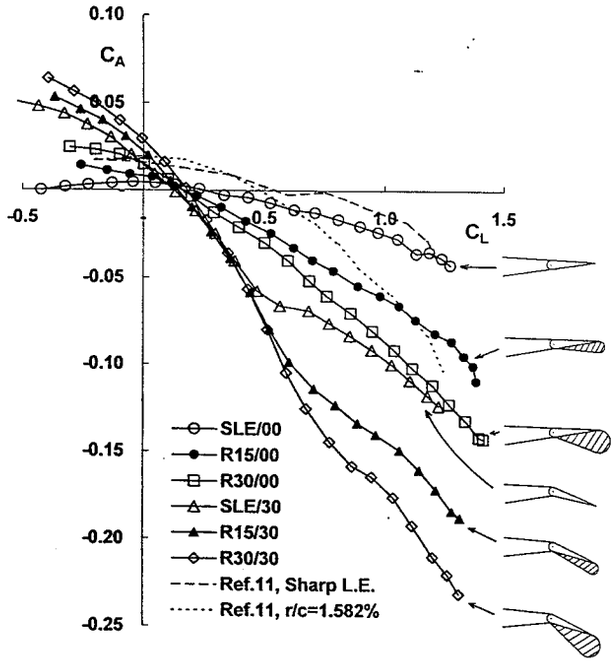

Fig.10 Axial Force C_A vs. C_L

K. FINOIE